

Matter Wave Isotope Separation in a Ring Trap

Sriganapathy Raghav¹, Suranjana Ghosh², Barun Halder¹,
Utpal Roy^{1*}

¹Department of Physics, Indian Institute of Technology, Patna,
801106, Bihar, India.

²Department of Physics, Indian Institute of Science Education and
Research, Kolkata, 741246, West Bengal, India.

*Corresponding author(s). E-mail(s): uroy@iitp.ac.in;

Abstract

We devise a novel mechanism of isotope separation from a mixture of Bose-Einstein condensate in the presence of interspecies interaction. Fractional revivals of this miscible system are studied inside a ring waveguide for spatially resolving the isotopes of ***Rb***. The characteristic time scale is influenced by the ring radius and the strength of interspecies interaction. We identify the physical parameters for which the autocorrelation function displays the signature of distinguishability. A study of the separability function further suggests favourable time instances for separating the isotopes with greater yields. The precise ranges of ring radius and interspecies interaction strength are revealed. We illustrate condensate densities at proposed time instances, which confirms our results and also validates our method.

1 Introduction

The natural abundances of isotopes are mostly in the form of mixtures. Often, a particular isotope is required in pure form and thus, isotope separation has been an enduring problem in science. Separation of stable isotopes involves methods such as diffusion or centrifugation [1], ion-exchange chromatography [2], light-induced drift isotope separation (LIDIS) [3, 4] etc., which rely on the difference in the isotopic mass, isotopic charge and isotopic shift in atomic or molecular spectral lines, respectively. The isotopes of the alkali metals can be separated from an isotopic mixture of Bose-Einstein

condensate (BEC), where phase separation is exploited by tuning the interspecies Feshbach resonance [5–7]. One could note that the regime of separation for the ground state of the two species lies at the greater values of the interspecies interaction [6, 8, 9]. This is because, at higher values of interspecies interaction, the energy of the inhomogeneous state is lower than that of the homogeneous state, which favours the spatial separation of the isotopes. The isotope separation is also predicted for a BEC mixture under the Thomas-Fermi limit [10–12]. Experimental observation of spatial separation is also achieved, but by neglecting the role of mass-imbalance between the isotopes [5]. The miscible-immiscible transition is shown in the absence of an external trap, where the transition is governed by the strength of the interspecies interaction in comparison to the intraspecies interaction [10].

On the other hand, the phase boundary of such transition is also shown to alter by changing the trap frequency [13–15]. The external trap, being the most favourable physical quantity to control the dynamics of a BEC, drives a quick emergence of various technological applications [16–18]. A large amount of literature exists towards the theoretical and experimental studies of efficient trap engineering in BEC [19–25]. A ring-shaped waveguide is one of the most useful traps in 2D, which is formed by overlaying a blue-detuned laser in the middle of harmonic confinement [26, 27], where the radius of the ring can be efficiently controlled. BEC inside such a ring waveguide manifests a number of interesting physics. The phenomenon of fractional revivals (FR) is recently reported in this system [28] and is a very well-studied effect in diverse quantum systems in their time evolutions [29–37].

In this work, we present a novel technique of isotope separation from the isotopic mixture of trapped Bose-Einstein condensates. The underlying model involves the dynamics of an isotopic mixture of a binary BEC inside the ring trap. The inclusion of interspecies interaction makes the FR-physics more rigorous and interesting due to the emergence of two time-scales, which are influenced by each other. We provide a systematic study of the time-evolution and identify the region of experimental parameters, the trap parameters and the interspecies interaction strength, for which the isotopes of Rubidium, ^{85}Rb and ^{87}Rb , will get spatially resolved. Employing FR of mixed BEC in a ring waveguide to spatially separate its isotopes will be the first-of-its-kind technique.

The paper is organized as follows. The next section deals with the model of interacting BEC mixture in a ring trap, along with the numerical technique to be adopted. Section III includes a detailed analysis of the combined dynamics through a modified FR phenomenon, where the influence of interspecies interaction on the individual time scales becomes apparent. A range of interspecies interactions is proposed in Sec.IV, which later suggests physical situations for isotope separation through autocorrelation function. In Sec.V, we quantify the degree of isotope separation at different time instances and identify the favourable situations for greater isotopic yields in experiments. A precise parameter domain is also revealed for ring radius and interspecies interaction. Visualization of condensate densities at the identified instances clearly manifests the spatial separation of the isotopes, which validates our model for practical applications. The paper concludes in Sec.VI with a summary and possible implications.

2 Basic Formulation of the System and the Method

We describe the method for the isotopic mixture of ^{85}Rb and ^{87}Rb BECs, having atomic masses m_1 and m_2 , number of atoms N_1 and N_2 , respectively. Both the components have their respective intra-species scattering lengths, a_{11} and a_{22} , whereas inter-species coupling is governed by the scattering length a_{12} and is tuned to the desired values through the inter-species Feshbach resonance [38–42]. The dynamics of a two-component BEC in a ring trap is described by the three-dimensional (3D) mean-field Gross Pitaevskii Equation (GPE), which is made dimensionless by scaling the position, time, and energy by a_\perp , $1/\omega_\perp$ and $\hbar\omega_\perp$, respectively. Here, $a_\perp = a_{1,\perp} = \sqrt{\hbar/2m_1\omega_\perp}$ is the harmonic oscillator length in the transverse direction when the ring trap is created in the x - y plane. ω_\perp is taken as $\omega_{1,z}$, the trap frequency as experienced by ^{85}Rb in z -direction. All the physical quantities are chosen as per the experiment [5, 39]: $N_1 = N_2 = 10^3$; $m_1 = 85$ a.u., $m_2 = 87$ a.u., $\omega_\perp = 2\pi \times 130$ Hz, $a_\perp = 0.675\mu\text{m}$; $a_{11} = a_{22} = 2.698 \times 10^{-9}$ m; and the radial frequencies, $\omega_r = \omega_{1,r} = \omega_{2,r}$ [5]. The GPE is written after dimensional reduction to quasi-2D as follows [43–45].

$$i\frac{\partial\psi_i}{\partial t} = [\mathcal{L} + \mathcal{N}]\psi_i, \quad (1)$$

where $\psi_i \equiv \psi_i(x, y, t)$ and $\mathcal{L} = -\frac{m_1}{2m_i}\nabla_{x,y}^2$ with $\nabla_{x,y}^2 = \frac{\partial^2}{\partial x^2} + \frac{\partial^2}{\partial y^2}$. The second term, $\mathcal{N} = \sum_{j=1}^2 g_{ij}|\psi_j|^2 + V_i(x, y)$, contains the tunable quantities, such as the couplings, $g_{ij} = \frac{\sqrt{2\pi}\lambda(m_1+m_2)a_{ij}N_j}{m_2a_\perp}$ and the ring trap,

$$V_i(x, y) = \frac{1}{4}\rho_i\omega^2(x^2 + y^2) + V_0e^{-\frac{2(x^2+y^2)}{\sigma^2}}, \quad (2)$$

which is a combination of a 2D harmonic potential and a Gaussian potential. Here $\rho_i = m_i/m_1$, $\omega = \omega_r/\omega_\perp$. σ and V_0 are the waist and amplitude of the Gaussian spike, respectively. The oscillations along the radial direction are suppressed by placing the condensate in the exact minimum (r_0) of the potential [46].

Numerical Method: We adopt the Split Step Fourier Method (SSFM) [47–49] for numerically solving the system, where both the parts of the dynamical equation (Eq.1) are treated separately. The first term is evolved in the momentum space, and the second term, involving the nonlinearity and the trap, is evolved in the coordinate space [47]. The x - and y -coordinates are equally divided into 512 grids with a step size of 0.1841. The step size for time is 0.0915 with a total of 16384 grids up to the second revival time.

3 Dynamics of the Condensate Mixture

We consider that the condensates of the two isotopes initially coexist in the form of a binary peak with waist, $d_0 = 0.75 a_\perp$, and at the diametrically opposite points of the ring with coordinates, $(\pm r_0, 0)$. The mixed cloud disperses along the ring waveguide

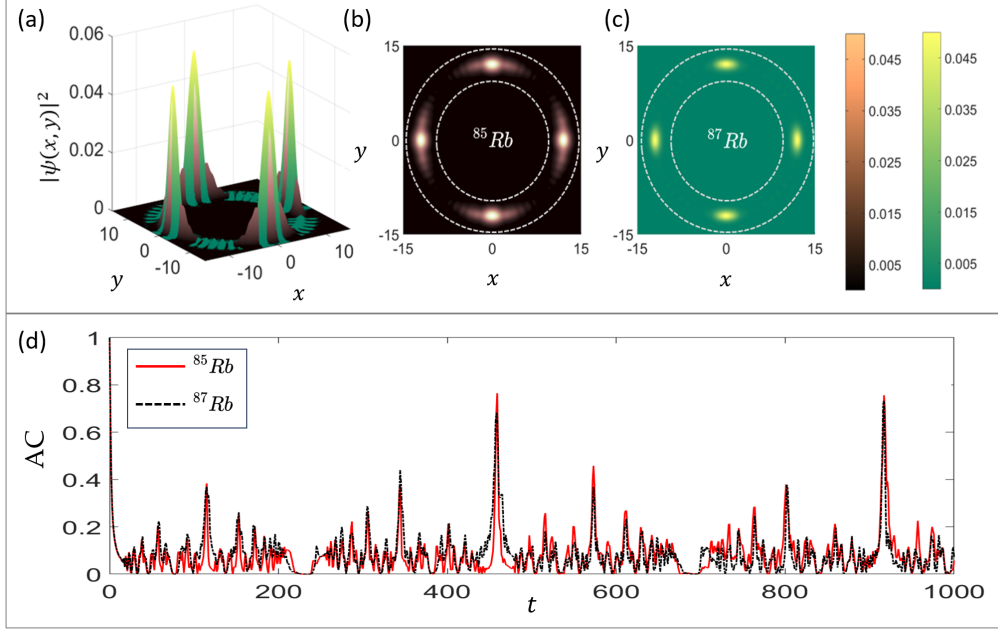


Fig. 1 (a) The density of the BEC mixture of ^{85}Rb and ^{87}Rb with interspecies interaction strength $a_{12} = 1.0 a_{11}$, at the quarter revival time, $t = T_R/4$. The densities of the two isotopes are shown separately in (b) and (c). The autocorrelation functions of the two interacting species are shown in (d). The ring radius is taken as $r_0 = 12a_{\perp}$. x and y are in the units of $a_{\perp} = 0.675 \mu\text{m}$ and, t is in the units of $1/\omega_{\perp} = 1.224 \text{ ms}$.

in clockwise and anti-clockwise directions. They will start interfering at $(0, \pm r_0)$, and also continue to spread further.

It is important to note that a single component BEC (not the system under study) in a ring trap, after some specific time interval, revives in its initial position and shape. The time when the condensate replicates the initial configuration is termed the revival time, T_R . This revival phenomenon has been thoroughly examined recently, where the exact revival time is given by $T_R = \pi r_0^2$ [28]. Moreover, at some specific fractions of this revival time ($t = T_R \times p/q$), several mini replicas of the initial condensate are formed, and this phenomenon is known as fractional revivals (FR), where p and q are mutually prime integers and decide the number of splits [28]. According to the model, at time $\frac{T_R}{4}$ ($p = 1, q = 4$), a single initial cloud will split into two, and a dual initial cloud will split into four daughter condensates. Moreover, two components of a binary BEC with no interspecies interaction will independently show FR and follow the above model, which is not the case for an isotopic mixture of BECs where interspecies interactions are considered.

To display the resultant cloud of the isotopic mixture in the presence of interspecies interactions, we choose a FR time as $T_R/4$ and the condensate is delineated in Fig.

1(a). It is apparent that the condensates of both the isotopes are mixed in a nontrivial manner due to their coexistence. This becomes further clarified when the condensate densities of ^{85}Rb and ^{87}Rb are shown separately in Fig.1(b) and 1(c), respectively. These densities look identical and not distinct, resulting in a miscible cloud, as shown in Fig. 1(a). To separate two constituent clouds of the interacting isotopes, we need to unwind the physics of miscibility and then try to devise a way. The well-known autocorrelation (AC) function helps us in the first stage. AC is the modulus square of the inner product of the initial and the temporally evolved wavefunctions, having mathematical definition as

$$|A(t)|^2 = \left| \int_{-\infty}^{\infty} \int_{-\infty}^{\infty} \psi^*(x, y, 0) \psi(x, y, t) dx dy \right|^2. \quad (3)$$

For a dispersing cloud, the AC function decays with time to manifest, gradually decreasing fidelity with the initial structure. However, the existence of significantly dominant peaks have different physics and are also observed in Fig.1(d) for the mixed cloud in Fig. 1(a). Periodic AC peaks with nearly one magnitude are the signature of revivals, whereas there are other periodic peaks of lower magnitudes, which are known as FR instances. Overall, the AC time-series provides us with comparable characteristic time scales for both the isotopic condensates in the presence of interspecies interactions, due to which the components remain indistinguishable.

Therefore, Fig.1(a) to Fig.1(d) suggest designing a physical situation when AC peaks will get separated in time during some FR instances to distinguish and measure two isotopic condensates from their mixture. The key physical parameters to control the dynamics are the radius of the ring trap (r_0), interspecies interaction (a_{12}) and time. It is clear from Fig.1 that the interspecies interaction, $a_{12} = 1.0 a_{11}$, and ring radius, $r_0 = 12a_{\perp}$, do not help in isotope separation during the whole temporal dynamics. Below, we will explore the influence of interspecies interaction on the individual revival dynamics of the isotopes.

3.1 Revival Dynamics of the Mixture without and with Interspecies Interactions

For a two-component BEC, we have two-time scales, one for each component. First, we will discuss about the expression for revival times of the two species at zero interspecies interaction. It is known that an initial Gaussian wave packet of two isotopes with width $w_{i,1} = w_{i,2} = w_i$, centred at $(r_0, 0)$, propagates along the ring and interferes with itself at $(-r_0, 0)$. The resulting interference maxima of the two species are proportional to the oscillating terms in their density [43] and are given by

$$\begin{aligned} I_{max,1} &\propto \cos \left(\frac{2Dtd}{w_i^2 w_{t,1}^2} \right), \\ I_{max,2} &\propto \cos \left(\frac{2m_1 Dtd}{m_2 w_i^2 w_{t,2}^2} \right), \end{aligned} \quad (4)$$

where $I_{max,1}$ and $I_{max,2}$ are the interference maxima of ^{85}Rb and ^{87}Rb , respectively. The condensates are initially separated by distance D at position d and with width w_i . $w_{t,1}$ and $w_{t,2}$ are their widths at a later time t . These widths are related by

$$w_{t,1} = \sqrt{w_i^2 + \left(\frac{2t}{w_i}\right)^2},$$

$$w_{t,2} = \sqrt{w_i^2 + \left(\frac{2m_1 t}{m_2 w_i}\right)^2}, \quad (5)$$

respectively. The difference in the interference maxima is brought out due to the difference in the revival times of the isotopes. Hence, we have different effective fringe separations for the two species:

$$\Delta d'_1 = \frac{4\pi t}{D}, \quad \Delta d'_2 = \frac{4\pi m_1 t}{m_2 D}.$$

At revival times, the fringe separation becomes $2\pi r_0 \times p$ due to the circular geometry of the ring, where p denotes the winding number. Since the initial separation D between the wave packets is $2\pi r_0$, the revival time for ^{85}Rb and ^{87}Rb are obtained as,

$$T_{R,1} = \pi r_0^2 \times p,$$

$$T_{R,2} = \frac{m_2}{m_1} \pi r_0^2 \times p. \quad (6)$$

The difference of the revival times of ^{85}Rb and ^{87}Rb in the absence of interspecies interaction becomes

$$\Delta T_R = \left(\frac{m_2}{m_1} - 1\right) \pi r_0^2. \quad (7)$$

It is clear from the above equation that the difference in the revival time scales for two noninteracting isotopes is merely due to the mass-imbalance of the two species. The solid line with squares in Fig. 2 shows ΔT_R with the radius of the ring in the absence of interspecies interaction. This variation is quite straightforward from the above analytical expression. However, the presence of interspecies interaction makes the variation quite nontrivial, and it doesn't follow Eq. 7. In this case, ΔT_R is plotted after numerically solving the dynamical equation and by finding the revival times for an interacting mixture, as depicted by the dotted lines with circles and triangles in Fig. 2 for two nonzero interactions, $a_{12} = 0.5a_{11}$ and $a_{12} = 1.0a_{11}$, respectively. The difference in the time scales of the mixed constituents is not significant enough without offering us quite a favourable situation for separating the isotopes. This also explains why we didn't have separation for $a_{12} = 1.0 a_{11}$ in fig. 1. The important points from Fig. 2 are i) the nonuniform time scale variation with the ring radius and ii) the possibility of influencing the time scale variation with respect to the different interspecies interaction strengths.

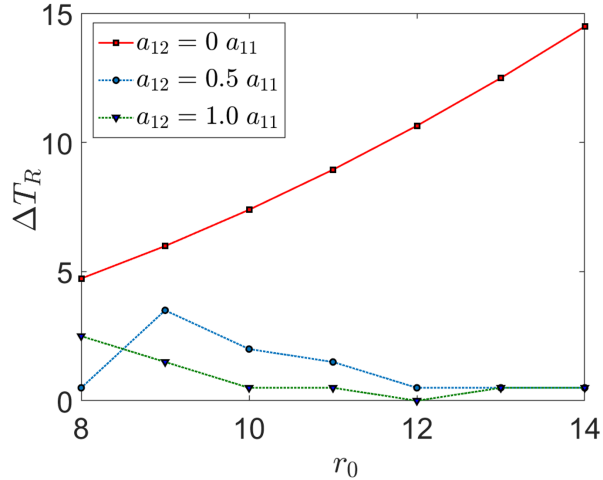


Fig. 2 Difference in the revival times of the two isotopes ΔT_R , for various radii are shown. The solid line with squares is in the absence of interspecies interaction, whereas the dotted line with circles and triangles is in the presence of interspecies interaction $a_{12} = 0.5a_{11}$ and $a_{12} = 1.0a_{11}$, respectively. Here, radius r_0 , revival time T_R , and interspecies interaction a_{12} are in the units of a_{\perp} , $1/\omega_{\perp}$, and a_{11} , respectively.

4 Identifying Appropriate Interspecies Interaction for Isotope Separation

We have seen that a mixture of isotopes with interspecies interaction doesn't follow Eq.[6] and both the isotopes have their revival times altered due to interaction strength for a given external trap. We evaluate the revival times of both the species for a wide range of interaction strengths with constant ring radii and depict them in Fig.(3). A merging of the time scales is observed at higher interspecies interactions. This behaviour is also seen for other fractional and revival times of the two species at greater interspecies interaction. We have shown the merging of timescales for ring radii $r_0 = 10a_{\perp}$, $r_0 = 12a_{\perp}$ and, $r_0 = 14a_{\perp}$, in the Fig.3(a), 3(b) and 3(c), respectively.

The interesting point to gain here is the wide difference in the time scales of the interacting species for a significant range of interspecies interaction. Moreover, the greater the radius, the greater the difference in the revival times at $a_{12} = 0$ as shown in Fig.2. This difference in the time scales is definitely the situation where the mixed condensate cloud should manifest a separation. The separation of isotopes is not possible for interspecies interaction strength $a_{12} \gtrsim 0.5a_{11}$, due to insignificant differences in the revival times of the two species. Therefore, for separating isotopes, one needs to choose 1) an interspecies interaction strength for which the revival times of the two species are fairly separated and 2) a ring radius for which the difference in the revival times, in the absence of the interspecies interaction strength, is considerably large. To examine whether such a situation is indeed favourable for separating the BEC of

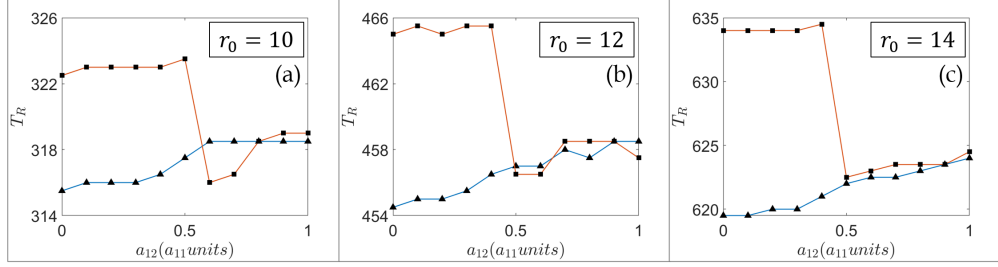


Fig. 3 Variation of revival time for ^{85}Rb (line with squares) and ^{87}Rb (line with triangles) with interspecies interaction a_{12} , for fixed ring radii, (a) $r_0 = 10a_{\perp}$, (b) $r_0 = 12a_{\perp}$ and (c) $r_0 = 14a_{\perp}$. Here, r_0 , T_R , and a_{12} are in the units of a_{\perp} , $1/\omega_{\perp}$, and a_{11} , respectively.

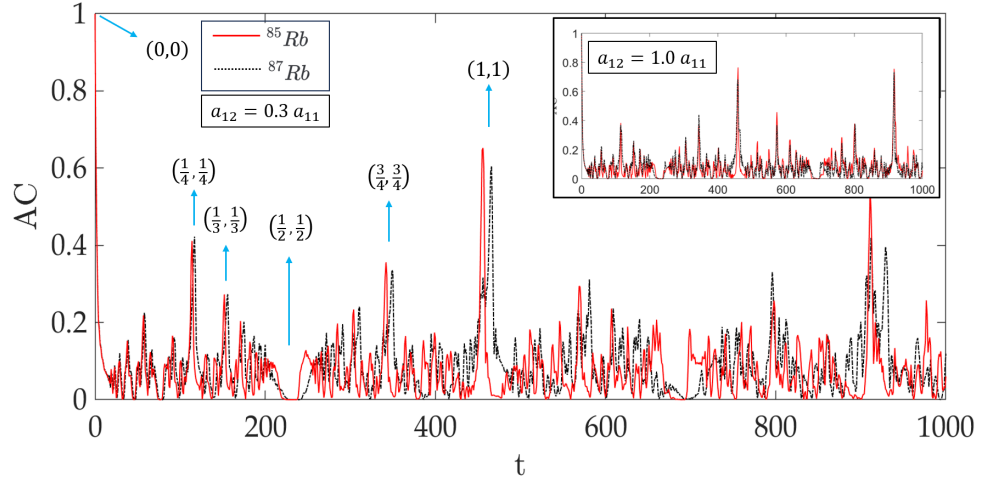


Fig. 4 Autocorrelation function of two initial condensates of a coupled BEC with interspecies interaction $a_{12} = 0.3 a_{11}$. Fractional revival instances are indicated by pair notations. The inset shows the autocorrelation function of the two species at $a_{12} = 1.0 a_{11}$ for comparison. The ring radius is taken as $r_0 = 12a_{\perp}$ and t is in the unit of $1/\omega_{\perp} = 1.224\text{ms}$.

two miscible isotopes, we choose a set of preferred parameters: $r_0 = 12a_{\perp}$ and interspecies interaction strength, $a_{12} = 0.3a_{11}$. We repeat the AC function plot with these parameters in Fig. 4 for ^{85}Rb (solid line) and ^{87}Rb (dotted line) interacting condensates, where every peak corresponds to a fractional revival time, and we compare it with the previous AC function (Fig.1(d)) plot, given in the inset of Fig. 4. AC peaks are seen to separate, unlike in the previous case. The FR times of both the species are indicated by the notation, (t_1, t_2) , such that $(\frac{3}{4}, \frac{3}{4})$ corresponds to $\frac{3}{4}^{\text{th}}$ revivals of both, ^{85}Rb and ^{87}Rb . The spacing of the peaks increases with time, thereby making

it possible to identify time instances where the difference in the AC functions of the two species is maximum. As discussed earlier, the greater the difference in the two AC functions, the lesser the spatial overlap between two isotopes. Two condensate wavefunctions will become distinguished or separately measured when the pair of peaks are separated from each other. In other words, the maximum of one AC peak should coincide with the minimum of the other AC peak. This, being a dynamical system, such typical situation has to be maintained for separation. The pair of peaks (1, 1) is one such instance. Hence, our methodology is indeed helpful in choosing the optimal values of r_0 and a_{12} for which the isotope separation is possible.

5 Separability of the Isotopes

From the autocorrelation functions of the two species, one could notice the separation of the isotopes. However, it requires careful analysis of how much they are separated and at what times for efficient implementation of the isotope separation scheme. To obtain the degree of separation, we define a quantity called 'Separability (S)' between the two isotopes in the mixed BEC:

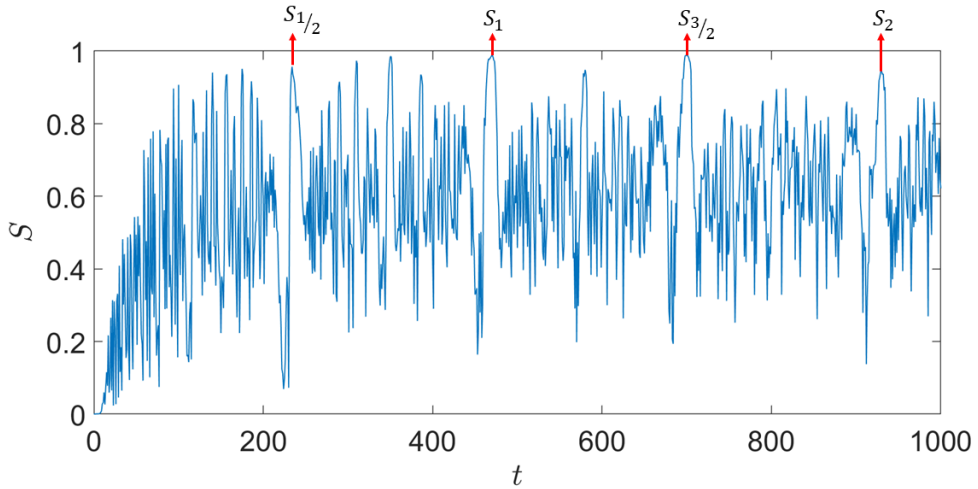


Fig. 5 Variation of the isotope Separability with Time. The prominent separability peaks are indicated, such as $S_{\frac{1}{2}}$ denotes the time near the 1/2-th fractional revival of ^{87}Rb . The inter-species interaction is taken as $a_{12} = 0.3a_{11}$ and the ring radius is $r_0 = 12a_{\perp}$. t is in the unit of $1/\omega_{\perp} = 1.224$ ms.

$$S = 1 - \Delta, \quad \Delta = \frac{[\int_{-\infty}^{\infty} \int_{-\infty}^{\infty} |\psi_1(x, y)|^2 |\psi_2(x, y)|^2 dx dy]^2}{\int_{-\infty}^{\infty} |\psi_1(x, y)|^4 dx dy \int_{-\infty}^{\infty} |\psi_2(x, y)|^4 dx dy}. \quad (8)$$

The term, Δ , is given by the square of the inner product of the probability densities of ^{85}Rb and ^{87}Rb , weighted by the product of 4th order moment of the inner product. The numerator helps in amplifying the tiny variations in the overlap of the wavefunctions of two species. The separability takes the value from 0 to 1, where 0 implies zero separation and 1 corresponds to a 100% separation. We choose the parameters of Fig. 4 for calculating S and presented in Fig. 5. A separability peak close to 1 will be the desired situation. For times up to 1000 in the unit of $\frac{1}{\omega_{\perp}}$, we could find four prominent peaks, $S_{\frac{1}{2}}$, S_1 , $S_{\frac{3}{2}}$ and S_2 , occurring closer to $\frac{1}{2}$, 1, $\frac{3}{2}$ and 2 of the revival time of ^{87}Rb . At these times, the separation of the isotopes is maximum, i.e., $S \approx 1$, compared to the other times.

The times corresponding to $S_{\frac{1}{2}}$, S_1 , $S_{\frac{3}{2}}$ and S_2 are $0.286s$, $0.575s$, $0.855s$ and, $1.138s$, respectively. At these times, the condensate densities of the two species have $> 95\%$ separation. The exact values of the percentage of separation of the two isotopes for the above Separability peaks are given in Table.1.

Peak	$S_{\frac{1}{2}}$	S_1	$S_{\frac{3}{2}}$	S_2
Time (s)	0.286	0.575	0.855	1.138
Separability	95.7%	98.9%	98.7%	94.5%

Table 1 Percentage of separation of the two isotopes for the four Separability peaks and their corresponding times from Fig. 5. The interspecies interaction is taken as $a_{12} = 0.3a_{11}$ and the ring radius is $r_0 = 12a_{\perp}$.

In addition, a more favourable instance will be relying on the following factors too: 1) at higher evolution time, one could observe an overall decay of the autocorrelation function (Fig.4) due to dispersion and hence, sooner is better for isotope separation; 2) a broader temporal width of the separability peak is preferable, as it will provide better time window in which the isotopes remains separated in the experiment.

Parameter Contours for Maximal Isotope Separation: In our work, the separability of the isotopes is tuned by two physical parameters, the radius of the ring r_0 and the interspecies interaction a_{12} . The separability peaks in Fig. 5 offers the times for maximal isotope separations, designated by $S_{\frac{1}{2}}$, S_1 , $S_{\frac{3}{2}}$ and S_2 and having $> 95\%$ isotope yields. The exact values of the percentage of separation are given in Table.1. These, along with the above points (1 and 2), suggest one of the most favourable instances as S_1 with a wider separability peak and 98.9% yield. We identify the parameter contours, comprising of r_0 and a_{12} , for the instance, S_1 , and depict it in Fig. 6.

The diagram highlights the regions above 90% separability. Though the whole highlighted region provides a wide parameter range for isotope separation, one can further improve it by choosing greater yields, as shown by different contours. The white dotted line in the middle indicates the maximum separability value for both parameters. It is interesting to note that the maximum separability line lies within the window $0.2a_{11} > a_{12} > 0.4a_{11}$ of interspecies interaction strength. We also draw the regions for various percentage yields, 90%, 95% and 98%, by dashed contours.

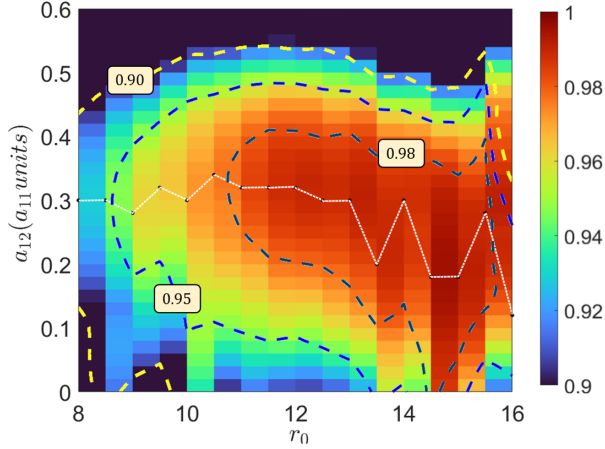


Fig. 6 The preferred parameter regions for isotope separation in experiments, following the Separability, S_1 , as an example. The interspecies interaction a_{12} and ring radius r_0 can be chosen as per the need, where the white dotted line indicates the maximum separability. We also draw the regions for various percentage yields, 90%, 95% and 98%, by dashed contours. The ring radius is in the unit of $a_{\perp} = 0.675 \mu\text{m}$, and the interspecies interaction is in the unit of $a_{11} = 2.698 \times 10^{-9} \text{ m}$.

For a desired separation line, the favourable values for the radius and interspecies interaction can be chosen in the experiments.

Condensate Densities Upon Isotope Separation: One can visualize the individual condensate of the isotopes for any set of parameters, described in the parameter contour plot in Fig. 6 to verify their spatial separation. Here, we will choose one of the values, such as the interspecies interaction is $a_{12} = 0.3a_{11}$ and the ring trap radius is taken as $r_0 = 12a_{\perp}$ in Fig. 7. Condensate densities of both the isotopes, ^{85}Rb and ^{87}Rb , separately plotted at times, 0.286 s, 0.575 s, 0.855 s, and 1.138 s, corresponding to $S_{\frac{1}{2}}$, S_1 , $S_{\frac{3}{2}}$ and S_2 , respectively. These instances, near multiples of half revival, do not further split the initially considered dual clouds and, hence, show nice separation in the preferred parameter window. At $S_{\frac{1}{2}}$, the isotopes are separated with respect to their common centre of mass and remain separated for a shorter time interval, as reflected from the narrow width of the separability peak for $S_{\frac{1}{2}}$ in Fig. 5. It is fascinating to observe that each of the other pairs of plots for ^{85}Rb and ^{87}Rb condensates in Fig. 7 manifests orthogonal positioning with respect to each other, implying a clear isotope separation inside the ring trap.

6 Conclusion

We have reported a method to separate isotopes from a mixed-binary BEC of Rb isotopes, which is made to evolve along a ring waveguide. The difference in the fractional revival time scales of the two interacting isotopes is employed in spatially separating them. We have quantified the degree of spatial separation of isotopes by a quantity

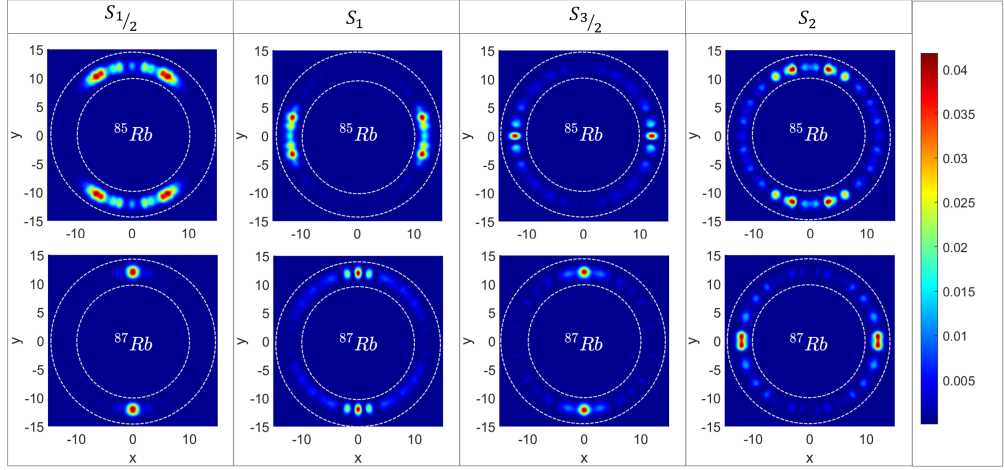


Fig. 7 Condensate densities of both the isotopes, ^{85}Rb and ^{87}Rb , separately plotted at times, 0.286 s, 0.575 s, 0.855 s, and 1.138 s, corresponding to $S_{\frac{1}{2}}$, S_1 , $S_{\frac{3}{2}}$ and S_2 , respectively. Spatial coordinates are in the units of $a_{\perp} = 0.675 \mu\text{m}$. The interspecies interaction is taken as $a_{12} = 0.3a_{11}$, the ring radius is $r_0 = 12a_{\perp}$ and time is in the unit of $1/\omega_{\perp} = 1.224 \text{ ms}$.

called Separability. The plot of separability and time gives us specific times when there is a maximum separation of isotopes. The times corresponding to $S_{\frac{1}{2}}$, S_1 , $S_{\frac{3}{2}}$ and S_2 are identified, where the condensate densities of the two species have $> 95\%$ separation. The percentage of separation is addressed up to $\sim 99\%$, which is higher than the previously reported isotope separation methods [4, 50] by using the LIDIS technique [4, 51–53]. The physically supported parameter contours offered a wide range of trap and cross-interaction values under the present scheme. The domain of inter-species interaction strength is unique ($a_{12} < a_{11}$) in the context of high fidelity spatial separation of isotopes in comparison to the past works [6, 8, 9].

References

- [1] De Groot, P.A.: Chapter 20 - Isotope separation methods, Handbook of stable isotope analytical techniques, 1025–1032 (2009)
- [2] Hosoe, M., Oi, T., Kawada, K., Kakihana, H.: Separation of rubidium isotopes by ion-exchange chromatography. Journal of Chromatography A **435**, 253–255 (1988)
- [3] Streater, A., Mooibroek, J., Woerdman, J.: Light-induced drift in rubidium: spectral dependence and isotope separation. Optics communications **64**(2), 137–143 (1987)
- [4] Streater, A., Mooibroek, J., Woerdman, J.: Enhanced efficiency in separation of rb isotopes by light-induced drift with the use of a diode laser with relaxation

sidebands. *Applied physics letters* **52**(8), 602–604 (1988)

[5] Papp, S., Pino, J., Wieman, C.: Tunable miscibility in a dual-species bose-einstein condensate. *Physical review letters* **101**(4), 040402 (2008)

[6] Wen, L., Guo, H., Wang, Y.-J., Hu, A.-Y., Saito, H., Dai, C.-Q., Zhang, X.-F.: Effects of atom numbers on the miscibility-immiscibility transition of a binary bose-einstein condensate. *Physical Review A* **101**(3), 033610 (2020)

[7] Kumar, R.K., Tomio, L., Malomed, B.A., Gammal, A.: Vortex lattices in binary bose-einstein condensates with dipole-dipole interactions. *Physical Review A* **96**(6), 063624 (2017)

[8] Wen, L., Liu, W.-M., Cai, Y., Zhang, J., Hu, J.: Controlling phase separation of a two-component bose-einstein condensate by confinement. *Physical Review A* **85**(4), 043602 (2012)

[9] Cikojević, V., Markić, L.V., Boronat, J.: Harmonically trapped bose–bose mixtures: a quantum monte carlo study. *New Journal of Physics* **20**(8), 085002 (2018)

[10] Ao, P., Chui, S.: Binary bose-einstein condensate mixtures in weakly and strongly segregated phases. *Physical Review A* **58**(6), 4836 (1998)

[11] Riboli, F., Modugno, M.: Topology of the ground state of two interacting bose-einstein condensates. *Physical Review A* **65**(6), 063614 (2002)

[12] Jezek, D., Capuzzi, P.: Interaction-driven effects on two-component bose-einstein condensates. *Physical Review A* **66**(1), 015602 (2002)

[13] Navarro, R., Carretero-González, R., Kevrekidis, P.: Phase separation and dynamics of two-component bose-einstein condensates. *Physical Review A* **80**(2), 023613 (2009)

[14] Merhasin, I.M., Malomed, B.A., Driben, R.: Transition to miscibility in a binary bose–einstein condensate induced by linear coupling. *Journal of Physics B: Atomic, Molecular and Optical Physics* **38**(7), 877 (2005)

[15] Sabbatini, J., Zurek, W.H., Davis, M.J.: Phase separation and pattern formation in a binary bose-einstein condensate. *Physical review letters* **107**(23), 230402 (2011)

[16] Bloch, I., Dalibard, J., Nascimbene, S.: Quantum simulations with ultracold quantum gases. *Nature Physics* **8**(4), 267–276 (2012)

[17] Ryu, C., Boshier, M.G.: Integrated coherent matter wave circuits. *New Journal of Physics* **17**(9), 092002 (2015)

- [18] Gajdacz, M., Opatrný, T., Das, K.K.: An atomtronics transistor for quantum gates. *Physics Letters A* **378**(28-29), 1919–1924 (2014)
- [19] Lesanovsky, I., Klitzing, W.: Time-averaged adiabatic potentials: versatile matter-wave guides and atom traps. *Physical Review Letters* **99**(8), 083001 (2007)
- [20] Henderson, K., Ryu, C., MacCormick, C., Boshier, M.: Experimental demonstration of painting arbitrary and dynamic potentials for bose-einstein condensates. *New Journal of Physics* **11**(4), 043030 (2009)
- [21] Nath, A., Roy, U.: Bose-einstein condensate in a bichromatic optical lattice: an exact analytical model. *Laser Physics Letters* **11**(11), 115501 (2014)
- [22] Raghav, S., Halder, B., Basu, P., Roy, U.: Tunneling and revival of anderson localization in a bose-einstein condensate. *Physical Review A* **106**(6), 063304 (2022)
- [23] Nath, A., Bera, J., Ghosh, S., Roy, U.: Exact analytical model for bose-einstein condensate at negative temperature. *Scientific Reports* **10**(1), 9016 (2020)
- [24] Halder, B., Ghosh, S., Basu, P., Bera, J., Malomed, B., Roy, U.: Exact solutions for solitary waves in a bose-einstein condensate under the action of a four-color optical lattice. *Symmetry* **14**(1), 49 (2021)
- [25] Basu, P., Halder, B., Raghav, S., Roy, U.: Nonlinear excitations in ultracold atoms trapped in triple optical lattices. *Condensed Matter* **7**(3), 52 (2022)
- [26] Ryu, C., Andersen, M., Clade, P., Natarajan, V., Helmerson, K., Phillips, W.D.: Observation of persistent flow of a bose-einstein condensate in a toroidal trap. *Physical Review Letters* **99**(26), 260401 (2007)
- [27] Naik, D., Raman, C.: Optically plugged quadrupole trap for bose-einstein condensates. *Physical Review A* **71**(3), 033617 (2005)
- [28] Bera, J., Ghosh, S., Salasnich, L., Roy, U.: Matter-wave fractional revivals in a ring waveguide. *Physical Review A* **102**(6), 063323 (2020)
- [29] Averbukh, I.S., Perelman, N.: Fractional revivals: Universality in the long-term evolution of quantum wave packets beyond the correspondence principle dynamics. *Physics Letters A* **139**(9), 449–453 (1989)
- [30] Robinett, R.W.: Quantum wave packet revivals. *Physics reports* **392**(1-2), 1–119 (2004)
- [31] Parker, J., Stroud Jr, C.: Coherence and decay of rydberg wave packets. *Physical review letters* **56**(7), 716 (1986)
- [32] Banerji, J., Ghosh, S.: The role of ro-vibrational coupling in the revival dynamics

of diatomic molecular wave packets. *Journal of Physics B: Atomic, Molecular and Optical Physics* **39**(5), 1113 (2006)

[33] Ghosh, S., Chiruvelli, A., Banerji, J., Panigrahi, P.: Mesoscopic superposition and sub-planck-scale structure in molecular wave packets. *Physical Review A* **73**(1), 013411 (2006)

[34] Ghosh, S., Roy, U., Genes, C., Vitali, D.: Sub-planck-scale structures in a vibrating molecule in the presence of decoherence. *Physical Review A* **79**(5), 052104 (2009)

[35] Roy, U., Ghosh, S., Panigrahi, P.K., Vitali, D.: Sub-planck-scale structures in the pöschl-teller potential and their sensitivity to perturbations. *Physical Review A* **80**(5), 052115 (2009)

[36] Ghosh, S.: Coherent control of mesoscopic superpositions in a diatomic molecule. *International Journal of Quantum Information* **10**(02), 1250014 (2012)

[37] Ghosh, S., Roy, U.: Enhanced quantum sensitivity in a vibrating diatomic molecule due to a rotational amendment. *Physical Review A* **90**(2), 022113 (2014)

[38] Burke Jr, J.P., Bohn, J.L., Esry, B., Greene, C.H.: Prospects for mixed-isotope bose-einstein condensates in rubidium. *Physical review letters* **80**(10), 2097 (1998)

[39] Papp, S.B., Wieman, C.E.: Observation of heteronuclear feshbach molecules from a ^{85}Rb - ^{87}Rb gas. *Physical Review Letters* **97**(18), 180404 (2006)

[40] Dong, S., Cui, Y., Shen, C., Wu, Y., Tey, M.K., You, L., Gao, B.: Observation of broad p-wave feshbach resonances in ultracold rb 85- rb 87 mixtures. *Physical Review A* **94**(6), 062702 (2016)

[41] Fukuhara, T., Sugawa, S., Takasu, Y., Takahashi, Y.: All-optical formation of quantum degenerate mixtures. *Physical Review A* **79**(2), 021601 (2009)

[42] Tanzi, L., Cabrera, C., Sanz, J., Cheiney, P., Tomza, M., Tarruell, L.: Feshbach resonances in potassium bose-bose mixtures. *Physical Review A* **98**(6), 062712 (2018)

[43] Pethick, C.J., Smith, H.: Bose-einstein condensation in dilute gases (2008)

[44] Adhikari, S.K.: Coupled bose-einstein condensate: Collapse for attractive interaction. *Physical Review A* **63**(4), 043611 (2001)

[45] Salasnich, L., Cardoso, W.B., Malomed, B.A.: Localized modes in quasi-two-dimensional bose-einstein condensates with spin-orbit and rabi couplings. *Physical Review A* **90**(3), 033629 (2014)

- [46] Zhang, X.-F., Kato, M., Han, W., Zhang, S.-G., Saito, H.: Spin-orbit-coupled bose-einstein condensates held under a toroidal trap. *Physical Review A* **95**(3), 033620 (2017)
- [47] Weideman, J., Herbst, B.: Split-step methods for the solution of the nonlinear schrödinger equation. *SIAM Journal on Numerical Analysis* **23**(3), 485–507 (1986)
- [48] Taha, T.R., Xu, X.: Parallel split-step fourier methods for the coupled nonlinear schrödinger type equations. *The Journal of Supercomputing* **32**(1), 5–23 (2005)
- [49] Wang, H.: A time-splitting spectral method for coupled gross–pitaevskii equations with applications to rotating bose–einstein condensates. *Journal of computational and applied mathematics* **205**(1), 88–104 (2007)
- [50] Okamoto, M., Nakamura, T., Sato, S.: Observation of light-induced drift effect of rubidium by using two diode lasers for pumping and re-pumping. *Materials transactions* **49**(11), 2632–2635 (2008)
- [51] Hradecny, C., Slovak, J., Tethal, T., Yermolayev, I., Shalagin, A.: Radioactive isotope and isomer separation using the light-induced drift effect. *International journal of radiation applications and Instrumentation. Part A. Applied radiation and isotopes* **43**(10), 1259–1264 (1992)
- [52] Hradecny, C., Tethal, T., Yermolayev, I., Zemlyanoi, S., Zuzaan, P.: Isotope separation of ^{22}Na and ^{24}Na by using the light-induced drift effect. *Applied radiation and isotopes* **45**(2), 257–260 (1994)
- [53] Yuki, K., Kobayashi, T., Matsuoka, L.: Numerical analysis of highly efficient laser-based method of radioactive cs isotope separation utilizing light-induced drift in d1 and d2 transitions in rare gases. *Journal of Nuclear Science and Technology* **54**(11), 1240–1250 (2017)